arXiv:1607.07476v2 [astro-ph.GA] 20 Mar 2017

Submitted to the Astronomical Journal

First lensed quasar systems from the VST-ATLAS survey: one quad, two doubles and two pairs of lensless twins

Paul L. Schechter[1]

MIT Kavli Institute for Astrophysics and Space Research, Cambridge, MA 02139

Nicholas D. Morgan

Staples High School, Westport, CT

B. Chehade

Durham University

N. Metcalfe

Durham University

T. Shanks

Durham University

Michael McDonald[1]

MIT Kavli Institute for Astrophysics and Space Research, Cambridge, MA 02139

ABSTRACT

We have analyzed images from the VST ATLAS survey to identify candidate gravitationally lensed quasar systems in a sample of WISE sources with $W1 - W2 > 0.7$. Results from followup spectroscopy with the Baade 6.5 m telscope are presented for eight systems. One of these is a quadruply lensed quasar, and two are doubly lensed systems. Two are projected superpositions of two quasars at different redshifts. In one system two quasars, though at the same redshift, have very different emission line profiles, and constitute a physical binary. In two systems the component spectra are consistent with the lensing hypothesis, after allowing for micro-lensing. But as no lensing galaxy is detected in these two, we classify them as *lensless twins*. More extensive observations are needed to establish whether they are in fact lensed quasars or physical binaries.

---

*This paper includes data gathered with the 6.5 meter Magellan telescopes located at Las Campanas Observatory, Chile.

[1]MIT Department of Physics

Subject headings: AGN: quasars — gravitational lensing: strong, micro

1. Introduction

Doubly and quadruply lensed quasar systems are valuable for widely disparate purposes. Treu and Marshall (2016) present a current survey of the use of time delay measurements for cosmography. The micro-lensing of lensed quasars can be used to determine sizes for the emitting regions of quasars (Rauch and Blandford 1991; Agol and Krolik 1999; Pooley et al, 2007; Blackburne et al 2011) and to measure the dark matter fraction in lensing galaxies (Schechter and Wambsganss 2004, Pooley et al 2012, Jimenez Vicente et al 2015). For each of these efforts the accuracy achieved is limited by the relatively small number of lensed systems.

The most productive lensed quasar discovery program to date has been the Sloan Digital Sky Survey Quasar Lens Search, henceforth SQLS (Inada et al. 2012), which yielded a statistical sample of 26 lensed quasar systems brighter than a limiting magnitude $i_{lim} = 19.1$ over 8000 square degrees in the redshift range $0.6 < z < 2.2$. An additional 36 systems that did not satisfy all of the selection criteria were also catalogued. Of 62 systems *in toto*, 40 were newly identified.

The ATLAS survey, carried out with VLT Survey Telecope (Shanks et al. 2015), promises to yield comparable if not greater numbers of lensed quasar systems. Its *ugriz* limiting magnitudes are nearly identical to those of SDSS. While its *ugriz* photometry covers only 4500 square degrees, the typical ATLAS seeing is 3/4 that of SDSS (Shanks et al. 2015), permitting the discovery of quasar pairs with smaller separations.

We have undertaken a search for lensed quasars in the ATLAS survey, and report here the first newly discovered lensed quasars: a quadruple system and two doubly lensed quasars. We also report two systems that have two nearly identical quasar spectra but for which no lensing galaxy has been detected.

In §2 we outline our method for identifying candidate lensed quasar systems, using the WISE catalog and ATLAS *ugriz* cutouts to choose candidates for spectroscopic and direct imaging followup. The method will be described in greater detail in a forthcoming paper. In §3 we describe direct imaging and spectroscopic followup observations of seven cadidate systems obtained with IMACS on the Baade 6.5 m telescope of the Magellan Observatory. In §4 we analyze these observations. In §5 we present simple models for the the newly discovered quadruple system, WISE 2344-3056 and for one of the doubles, WISE 2304-2214. We discuss our method and results in §6 and summarize our findings in §7.

2. Selection of Candidate Lensed Quasar Systems

2.1. Colors for marginally resolved lensed quasar systems

The colors derived for an object from a survey like ATLAS involve a number of implicit assumptions. Bright objects that are deemed point sources are used to determine a point spread function (PSF) appropriate to the exposure, usually dominated by the atmospheric seeing. Sources that appear extended with respect to this PSF might be fit with a Sersic (1963) profile. For sources that do not appear to be extended, one uses the adopted PSF to calculate a magnitude.

A gravitationally lensed quasar system is a composite object consisting of multiple images of a quasar and one or more lensing galaxies. Typical image separations are $\sim 1''$, to within a factor of two. It is unfortunate that the typical seeing in a survey like ATLAS is also of order one arcsecond. Were it very much better, one would detect the components of the lensed quasar as distinct objects and compute colors for each. Were it very much worse, one might treat the system as a point source.[1]

When the resolution of a survey is *comparable* to the image separation, the magnitudes derived for composite systems suffer systematic errors from the mismatch between the assumed PSF and the object. Moreover these systematic errors will vary with the seeing. While one might hope to select lensed quasars using their catalogued colors, systematic errors may cause systems to be missed.

The resolution of the WISE survey (Wright et al. 2010) is substantially worse than that of ATLAS, and WISE magnitudes for all but the widest lensed quasar systems do not suffer from marginal resolution. Our approach is therefore to make a first level selection based only on WISE colors. This produces a candidate list sufficiently small that one can then retrieve the ATLAS survey images for each remaining object and determine whether they are consistent with its being a system of two or more sources. Magnitudes are then computed by adopting a fixed configuration, with the same number of components, for all filters, thereby mitigating the systematic errors associated with marginally resolved systems.

2.2. W1 - W2 color selection

Stern et al (2012) have shown that the WISE $W1 - W2$ color ($m_{3.6\mu} - m_{4.5}\mu$) can be used to isolate quasars from stars, and, to a lesser extent, from galaxies. The underlying explanation is that the optical light from a quasar is thermal emission from an extended region with a range of temperatures, in which case the red tail of the distribution is redder than a blackbody Rayleigh-

[1]One might in principle convolve survey images with a broadening function, perhaps blurring those taken in different filters to a common PSF, and produce a catalog for the smeared data, but only with the expenditure of considerable resources.

Jeans spectrum, which has $W1-W2 \approx 0$ in the Vega system. We adopted a criterion, $W1-W2 > 0.70$, that struck a balance between including lensed quasar systems and isolating them from other objects. Eighty percent of the confirmed SQLS lensed quasar systems satisfy this criterion. Lensing galaxies have bluer $W1-W2$ colors than quasars. Systems in which the light from the lens dominates that of the quasars will not be included in our sample. The fraction of SQLS quasar systems that are bluer than our criterion is larger for the fainter systems. To keep the number of candidates manageable, we limited our sample to objects with $W1 < 15$ or $W2 < 14.45$.

In the south galactic cap, ATLAS covers a region with $21^h30^m < \mathrm{RA} < 4^h00^m$ and $-40^\circ < \mathrm{Dec} < -10^\circ$ in the *ugriz* filters with $0\farcs213$ pixels. (Shanks et al 2015). In the north it covers a region with $10^h00 < \mathrm{RA} < 15^h30^m$ and $-20^\circ < \mathrm{Dec} < -2.5^\circ$.[2] The completed survey will include 4292 fields, each one degree square, located on $0\fdg98$ centers. As of mid-March 2016 there were 3650 fields for which data in *u*,*g* and two or more of *r*,*i* and *z* were available.

ATLAS survey data in at least one filter was available, as of mid-March 2016, for 144,700 unique sources that satisfied our WISE criteria.

2.3. Cutouts

For each source in the overlap between WISE and ATLAS we downloaded $12''$ square *ugriz* FITS subrasters (58 pixels on a side) from the University of Edinburgh Wide Field Astronomy Unit's OmegaCam Science Archive (henceforth OSA; Hambly et al 2008; Cross et al 2012). The size of these "cutouts" was chosen to be larger than most known quasar/galaxy lens systems while minimizing the possibility of including an unrelated source in the field.

2.4. Splitting blended images

For each source the available cutouts were analzyed with a program that incorporates many of the core subroutines from the `DoPHOT` photometry program (Schechter, Mateo and Saha 1993). `DoPHOT` uses an elliptical profile that approximates a Gaussian near the core but has broader wings.

In each of the three filters with the best seeing, as recorded in the FITS header of the cutout, we attempt to split candidates into two sources with a common quasi-Gaussian shape. From these we chose the two source fit that shows the greatest improvement over a single extended object (as measured by our goodness of fit parameter) as our "anchor" estimate of the separation between components.

[2]A second northern region with $10^h00^m < \mathrm{RA} < 15^h00^m$ and $-35^\circ < \mathrm{Dec} < -20^\circ$ is being surveyed in *i* and *z*, with *u*, *g*, and *r* being observed in a separate ESO program (095.A-0561, PI L. Infante), but was not included in the present search.

For as many of the *ugriz* filters as we have cutouts, we carry out two source fits, with the separation constrained to our anchor value, but allowing the fluxes to vary along with a common set of shape parameters and an overall position. We call these constrained separation fits.

If the flux ratio from one of these constrained separation fits is very different from the anchor value (3 magnitudes) at a high level of significance (10σ) we take the anchor splitting to be spurious. This frequently happens at smaller separations, at which trailed or astigmatic images can cause the object to look elongated or double in one exposure.

2.5. Weeding out galaxies

In addition to quasars, our WISE quasar-colored systems include star forming galaxies, which often come in close pairs. Moreover, with a thousand unlensed quasars for every lensed quasar, we expect accidental projections of foreground galaxies close to quasars.

Every constrained separation fit gives us an elliptical footprint that can be compared with the seeing as recorded in the FITS header for that filter. Pairs of galaxies are expected to have larger footprints, as measured by the area of the quasi-Gaussian, than the stellar PSF. After some experimentation, we decided to eliminate as a probable galaxy pair any system for which the *area* of the constrained separation footprint is larger than that of the stellar PSF by 2 pixels in all three of the filters with the best seeing.

We carry out a second test using the cutout that yielded our anchor splitting, fitting for two sources whose shapes are not constrained to the same elliptical Gaussian. This adds three additonal shape parameters, but the fits converge for roughly 65% of our candidates.

We exclude systems for which the minor axes of the two components differ by more than than a factor of $\sqrt{2}$. We reason that while our splitting might lump together a close pair of quasar images, or a quasar image and the lensing galaxy, the minor axis of the fitted ellipse ought not to be much larger than the PSF of a star. But instead of using a nominal PSF, we use use the fit to the other split component. We further ighten this criterion if the major axis of the wider component is very much larger than the narrower one, excluding systems for which the minor axes differ by more than a factor of $2^{1/4}$ and for which the ratio of the areas is larger than a factor of two.

2.6. Ranking on the basis of achromaticity

The word "achromatic" is often used to describe gravitational lensing. While color may vary from one part of an extended source to another, if the source is small compared to the Einstein ring of a gravitational lens, the multiple images will all have the same color.

This is less powerful than one might hope in discriminating between lensed quasar systems

and chance superpositions of objects for two reasons. First, lensed systems also include lensing galaxies, the light from which will be split disproportionately between the two images. Second, especially at brighter apparent magnitudes, the quasars are micro-lensed by the stars within the lensing galaxies and are somewhat extended compared to the micro-lensing Einstein rings. This leads to differential micro-lensing (Blackburne et al 2011).

We use the constrained separation flux ratios at each observed wavelength, expressed in magnitudes, δm_λ, to fit for a slope, $d\delta m_\lambda / d \log \lambda$. We adopt a rough guess of the mean slope for a lensed system $< \alpha >= 0.217$, and of the scatter in that slope, $\sigma_\alpha = 0.325$, and score systems based on their deviation from the mean slope.[3] We also score systems on the absence of scatter from the observed slope and finally score systems on the consistency of the u filter flux ratio with those in the other filters. A final ranking is computed by taking the geometric mean of these three scores. Details of our scoring system (which we continue to refine as we observe more candidates) will be presented in a forthcoming paper.

2.7. Optical colors

We have argued above that catalogued optical colors may be unreliable for lensed quasar systems because catalog photometry explicitly or implicitly assumes a light distribution over the detector pixels that is inappropriate for a lensed quasar system. Our constrained separation model should produce better (but hardly perfect) colors.

For this, our first pass through the data, we restricted ourselves to the simplest of quasar color criteria, ultraviolet excess (henceforth UVX). This works well for quasars with $z < 2.2$ (Richards et al 2001) but would exclude the roughly 25% of unlensed quasars in an SDSS-like survey that have higher redshifts.

Optical colors were computed adding the two fluxes from the constrained separation fits in each of the filters. The photometric zeropoints embedded in the OmegaCam FITS headers were used to create $u-g$ colors in a Vega-like $ugriz$ system (Shanks et al 2015). We ultimately adopted $u-g < -0.5$ as our UVX criterion, which seems to exclude narrow emission line galaxies and white dwarf pairs, but to include lensed quasars at $z < 2.2$.

Applying the recipe described in this section, we are left with a ranked list of candidate lensed quasar systems.

---

[3]The mean slope is non-zero because fainter images are more likely to include more of the red light from the lensing galaxy.

3. Spectroscopic and Direct Observations and Reductions

From June 2015 through April 2016, and again in November 2016 spectroscopic observations were carried out for roughly a dozen highly ranked systems with both the f/2 and f/4 cameras of the Inamori Magellan Areal Camera and Spectrometer, henceforth IMACS (Dressler et al 2010) on the Baade 6.5-m telescope of the Magellan telescopes. In Table 1 we give coordinates for eight of the objects observed, their rankings and colors, and descriptions of the resulting spectra.

3.1. Choice of Systems

While guided by rank, the actual choice of systems to observe also depended upon seeing, as some of the systems are quite close, and upon cloud cover. Pairs of blue stars and narrow line galaxies with $-0.5 < u - g < 0$ that predominated in our first observations led us to tighten our UVX criterion to $u - g < -0.5$ in subsequent runs.

3.2. Direct Imaging of WISE 2344-3056

The system WISE 2344-3056 was given top priority for observation in December 2015 because its appearance in the ATLAS images suggested a quadruple system. Figure 1 shows the VST ATLAS image of WISE 2344-3056 in the g filter, which gave the best splitting of the object. We have superposed the elliptical FWHM contours from the anchor fit to this image.

The minor axis of the anchor fit is $1\farcs11$, slightly less than the $1\farcs18$ seeing reported in the image header. The major axis is $1\farcs41$ and elongated so that each ellipse includes two of the four images.

The system only barely survived being eliminated as a pair of galaxies, suggesting that we may need to relax the constraint on the area of the anchor footprint described in §2.5.

The spectrocopic mode used with IMACS required the taking of one or more short direct images to position the object in the slit. The first of those obtained for WISE 2344-3056, in Sloan r, confirmed the suspicion that it was at least triple so two more images were taken in Sloan i. The left panel of Figure 2 shows one of the i images, taken in $0\farcs55$ seeing with the f/2 camera.

The debiased and flatfielded frames were analyzed using the program `DoPHOT` (Schechter et al 1993). The standard version of the program found all four quasar images on the r frame and needed only minor nudging to find all four on the other two. The right panel of Figure 2 shows the residuals from one of those fits, using the point spread function of a nearby star as the empirical PSF. While the residuals show little or no trace of a lensing galaxy, the figure is somewhat deceptive. If one allows for a *fifth* point source with its position fixed at the expected position of the lens (see §5 below), the magnitudes of the four quasar images decrease by hundredths of a magnitude, the positions spread out radially by roughly 0.1 pixel each, and the flux from the hypothesized fifth

image is 1.5 ± 0.5 magnitudes less that of image D.

Astrometry was carried out on one of the i frames using catalogued positions from the ATLAS survey, with rms residuals of $0\farcs1$. Results are given in Table 2. The four positions are indicated by the blue circles in Figure 1.

Fluxes relative to the brightest image were likewise computed using `DoPHOT`. These were then used to compute magnitudes assuming a combined Petrosian i magnitude of 19.15 as given in the ATLAS catalogue, which reports magnitudes in an AB system (Shanks et al 2015) rather than in the Vega-like system of the FITS headers. To the extent that the quasar has varied in the 4 years between the ATLAS and IMACS exposures, these will share a common systematic error.

3.3. Direct Imaging of WISE 0326-3122

A 30 s direct image of WISE 0326-3056 in the Sloan r filter in $0\farcs64$ seeing was obtained with the IMACS f/2 in acquiring the object for spectroscopy. The debiased and flatfielded frame was analyzed with `DoPHOT`. Figure 3 shows the original image of the candidate system and the same image with best fitting PSFs subtracted. The residuals show little or no trace of a lensing galaxy. In contrast to the case of WISE 2344-3056, the residuals are not deceptive. If one allows for a *third* point source with its position fixed near he expected position of the lens (one third of the way from the fainter image to the brighter image) one gets a *negative* flux with an amplitude only 1% that of the fainter image. This limit is sensitive to the assumed position for the lens, which as we see in the case of WISE 2304-2214 below, can be quite different from the expectation.

3.4. Direct Imaging of WISE 2304-2214

In setting up for spectroscopy of WISE 2304-2214 a 30 s acquisition image in the Sloan r filter was obtained in $0\farcs63$ seeing with the IMACS f/4 camera binned 2×2. There appeared to be a lensing galaxy in between two pointlike images so a 60s image in the Sloan i filter was obtained following spectroscopy. Both exposures were analyzed by fitting two scaled versions of a stellar template and a quasi-Gaussian. The separations determined from the i exposure were enforced on the r exposure.

Figure 4 shows the original Sloan i image, the same image with all three sources subtracted, at 10 times the contrast, and again with only the two point sources subtracted at 4 times the contrast. We take the central object to be the lensing galaxy. The scale is $0\farcs221$ per pixel.

In Table 3 we give positions and magnitudes for all three sources. The latter are derived from the catalogued ATLAS magnitudes for the stellar templates, two of which were used for each filter. The quasi-Gaussian fit yields shape paramters for the lensing galaxy. We deconvolve that quasi-

Gaussian using a similar fit to the template star and find the semi-major and semi-minor axes to be 0.58 and 0.25 pixels respectively, at position angle $-68.^{\circ}6$, which is $9.^{\circ}5$ off the pependicular to the line connecting the two images. Similar results were obtained from the r exposure. It is noteworthy that contrary to the expectation for simple isothermal sphere models the lensing galaxy is closer to the brighter image. In this regard it is similar to the case of HE1114-1805 discussed in §4.1 below.

3.5. Spectra

Spectra for the objects in Table 1 were obtained using either the "short" f/2 camera or "long" f/4 camera on IMACS, in both cases using a 3800-7000 Å blocking filter. Dispersers with 300 lines mm^{-1} were used on both cameras: a grism blazed at $17.^{\circ}5$ on the short camera and a grating blazed at $4.^{\circ}3$ on the long camera. On the short camera the spectra were binned by 2 pixels in the spectral direction (except where noted). On the long short camera they were binned by 4 pixels in the spectral direction and 2 pixels (with one exception) along the slit. The $0.9''$ slit was oriented to obtain spectra of both components of the double systems.

The spectra were bias-subtracted and flattened using standard procedures, and cosmic rays near the extraction paths were identified by eye and replaced with interpolated values along each row of the detector. Wavelength calibration was provided by Argon lamp lines taken during the afternoons. A multi-order polynomial fit as a function of both the spatial and dispersion directions was used for the wavelength solution and gave typical fit rms values with respect to the reference line list of 0.3 Å or better for all target chips. The dispersion ranged from 2.2 to 2.6 Å $pixel^{-1}$ on the short camera and from 2.8 to 3.0 Å $pixel^{-1}$ on the long camera. Sky background was subtracted using linear interpolation along each row of the detector. The spectra show gaps near 6550 Å on the short camera and near 5300 Å on the long camera due to the physical spacing between CCDs on the IMACS cameras.

When the seeing permitted, spectra were extracted for the individual components of each system. The was accomplished by fitting multiple overlapping Gaussian profiles to each spatial row of the detector. We performed a preliminary fit for each row to obtain average component separations, and then a final extraction where the overall position, common FWHM, and component brightnesses were allowed to vary but the relative separations were fixed at the average values.

Figures 5-7 show the extracted spectra for the objects in Table 1; note that no flux calibration was performed. The displayed spectra were top-hat smoothed using a 3 pixel window in the dispersion direction for cosmetics. Gaussian profile fitting was performed on the unsmoothed spectra and we plot the base-10 log of our fitted Gaussian profile areas along the ordinate. We were able to extract individual spectra for WISE 0145-1327, WISE 0326-3122, WISE 1051-1142, WISE 1427-0715, WISE 2215-3056, WISE 2304-2214 and WISE 2329-1258. For these systems an inset at the lower right of each plot shows the Gaussian decomposition of the two components for a single CCD row of the detector. The small separation of WISE 2344-3056 precluded decomposing

the spectra, so a single Gaussian was used to extract the combined spectrum.

4. Interpretation of Spectra

4.1. Binary quasar, lensed quasar, or lensless twins?

The words "binary quasar" are used to describe two distinct quasars at the same redshift, as opposed to two images of a single lensed quasar (Hennawi et al 2006). But when one observes a pair of quasars, conclusive discrimination between these two alternatives is not always straightforward (Wisotzki et al 1993; Kochanek et al 1999; Mortlock et al 1999).

The history of HE1104-1805 is instructive in this regard. Wisotzki and collaborators (1993) found that the two components differed in the slopes of their continuua and in the equivalent widths of their emission lines, but that the shapes of their emission lines were identical. They argued that the spectral differences might be due to micro-lensing by stars in the lensing galaxy. But they detected no lensing galaxy at $R \lesssim 24$. Wisotzki et al (1995) subsequently observed correlated changes in the continuum flux of the two systems, which they took as confirmation of the lensing hypothesis. Courbin et al (1998) conclusively detected the lensing galaxy, much closer to the brighter image than might naively have been expected. Crude interpolation between filters in subsequent HST observations (Remy et al 1998) would give $R \sim 22$ for the lensing galaxy. Lidman et al (2000) measured a lens redshift of $z = 0.729$.

The circumstances of two of our systems are similar to those of HE1104-1805 in 1993. The spectra differ, but no more than they might under the micro-lensing hypothesis. Still, we observe no lensing galaxy. We think it premature to call such systems binary quasars, and instead refer to them as "lensless twins." If lensing galaxies or correlated variations are ultimately observed, they will be classified as lens systems.

But if only upper limits can be measured for a lensing galaxy, careful modeling is needed to establish that those upper limits are inconsistent with plausible lensing scenarios. Alternatively, higher signal-to-noise spectra or spectra of narrow emission lines might show significant differences in the line profiles or redshifts, ruling out the lensed system hypothesis.

In the sequel to the SQLS, the SDSS-III BOSS Quasar Lens Survey, More et al (2016) are similarly circumspect in not drawing strong conclusions about lensless twins for which no lensing galaxy is observed.

4.2. WISE 0145-1327: a projected pair

WISE 0145-1327 is a chance projection of two quasars. The brighter of the pair is at a redshift of $z = 1.0902 \pm 0.0005$ from a Gaussian fit to the MgII emission line. The fainter object is at a

higher redshift of $z = 1.9749 \pm 0.0005$ based on its CIV broad emission line. The spectra are shown in Figure 5.

4.3. WISE 0326-3122: lensless twins at $z = 1.34$

The two quasar images of WISE 0326-3122 have nearly identical redshifts and spectral flux ratios. Both show a CIII] broad emission line at around 4460 Å. Gaussian fits to the CIII] profiles yield identical source redshifts of $z = 1.3342 \pm 0.0016$ for the brighter object and $z = 1.3336 \pm 0.0026$ for the fainter object. This redshift places the MgII broad emission line inside the IMACS chip gap with only a hint of the feature's wing visible for the brighter component. There is also a MgII $\lambda\lambda$2796,2803 absorption doublet at $z = 0.5080 \pm 0.0001$ present in the brighter component's spectrum. The flux ratio between components is also remarkably constant at about 3.2:1 (0.5 dex in Figure 5) over the entire IMACS spectral range. This makes it all the more surprising that no lensing galaxy is observed in the PSF subtracted image (Figure 3). We take the two sources to be lensless twins.

4.4. WISE 1051-1142: lensless twins at $z = 0.88$

The two quasar images of WISE 1051-1142 have nearly identical redshifts. The single prominent emission line just blueward of the IMACS chip gap is likely MgII due to the absence of other emission features in the observed wavelength range. Gaussian fits to the emission profiles yield source redshifts of $z = 0.8839 \pm 0.0002$ and $z = 0.8811 \pm 0.0008$ for the brighter and fainter components, respectively, which overlap at the 3-4σ level. There are no obvious signs of intervening absorption. The flux ratio between components varies from 6:1 at the blue end to 7:1 at the red end, not inconsistent with wavelength-dependent continuum microlensing seen in other lensed quasars. We take the two sources to be lensless twins.

4.5. WISE 1427-0715: a projected pair

WISE 1427-0715 is a chance projection of two quasars. The brighter component shows the MgII broad emission line at about 6230 Å yielding a source redshift of $z = 1.2258 \pm 0.0004$. The only prominent emission line at 4820 Å in the fainter component is likely MgII due to the absence of other features in the observed wavelength range, yielding a source redshift of $z = 0.7218 \pm 0.0004$. A MgII $\lambda\lambda$2796,2803 absorption doublet is also seen in the brighter component's spectrum at a fitted redshift of $z = 0.7205 \pm 0.0004$ and thus associated with the host galaxy of the fainter quasar. The spectra are shown in Figure 6.

4.6. WISE 2215-3056: a binary quasar at $z = 1.34$

WISE 2215-3056 is a binary quasar. Its components have similar redshifts but have notable spectral differences. The brighter component is at $z = 1.3474 \pm 0.0003$ based on its MgII broad emission line profile and shows strong absorption features blueward of its CIII] and MgII emission lines. The fainter component has a source redshift of $z = 1.3508 \pm 0.0004$ based on its MgII profile, a $> 5\sigma$ difference from the brighter component, but shows neither of the two absorption features seen in the brighter component. There is also a prominent FeIII/UV 48 broad emission line of comparable intensity to CIII] in the brighter component that is lacking in the fainter companion. Despite the similar redshifts, the spectral differences argue for two separate quasars. The spectra are shown in Figure 6.

4.7. WISE 2304-2214: a doubly lensed quasar at $z = 1.42$

WISE 2304 -2214 is a doubly lensed quasar at z=1.423. The quasar spectra shown in Figure 6 have emission at CIII], CII] and MgII. Gaussian fits to the MgII emission profiles yield source redshifts of $z = 1.4222 \pm 0.0004$ and $z = 1.4218 \pm 0.0003$ for the brighter and fainter components, respectively. The brighter component has an MgII absorption doublet at $z = 0.6362 \pm 0.0001$ that is much weaker, if not totally absent, in the fainter component. Fitting a third Gaussian component of the same width between the two quasar components yields a spectrum of what appears to be the lensing galaxy with Ca H&K absorption near 5700Ågiving $z_{gal} = 0.4455 \pm 0.0004$.

The emission line equivalent widths are substantially smaller in the brighter component, suggesting that one or both components are micro-lensed. We make a crude estimate of emission line flux ratios by comparing the peak flux in the emission line to the flux in the adjacent continuum. We get emission line flux ratios of $B/A = 0.99$ for the C III] line and and $B/A = 1.06$ for the Mg II line.

4.8. WISE 2329-1258: a doubly lensed quasar at $z = 1.31$

The two quasar images of WISE 2329-1258 have nearly identical redshifts with a rich set of absorption features present in both spectra, as shown in Figure 7. The MgII broad emission line is at $z = 1.3077 \pm 0.0008$ for the brighter component and $z = 1.3174 \pm 0.0018$ for the fainter component, overlapping at the 5σ level. A similar agreement is seen for the CIII] broad emission line. The narrow-line absorption features present in the spectra of both components can be modeled with two absorbers at $z = 1.1525 \pm 0.0002$ and $z = 0.7644 \pm 0.0004$. Both are anchored by an appropriately redshifted MgII $\lambda\lambda$ 2796,2803 doublet and accompanying FeII $\lambda\lambda$2382, 2600 absorption lines. We also identify FeII $\lambda\lambda$2344, 2374 and 2586 for the $z = 1.1525$ absorber. The flux ratio between the components is also remarkably constant at about 2.5:1 (0.4 dex in Figure 7) over the entire IMACS

spectral range.

Based on the Magellan data presented here, WISE 2329-1258 would be classified as a lensless twin system. But Treu et al. (2017, private communication) have observed it using NIRC2 on Keck-II behind adaptive optics and detected the lensing galaxy as well as the lensed quasar host galaxy, so we count it as a confirmed lens. Like HE 1104-1805, this system also has strong absorption line systems, and we would not be surprised if one of these turns out to be the lens redshift.

4.9. WISE 2344-3056: a quad at $z = 1.30$

The slit used to obtain a spectrum for WISE 2344-3056 ran along the line connecting the ellipses in Figure 1, with light from all four images overlapping on roughly six spatial pixels. We present only the combined spectrum in Figure 7. The quasar redshift is $z = 1.2978 \pm 0.0003$ based on a Gaussian fit to the MgII broad emission line. The CIII] broad emission line is also present at a much lower signal to noise. There is at least one intervening absorption system at $z = 0.9472 \pm 0.0012$ anchored by the MgII $\lambda\lambda$2796,2803 absorption doublet, several FeII lines ($\lambda\lambda$2344,2374,2382,2399,2586,2600), FeIII λ2419, and MgI λ2852.

5. Lens models

We used Keeton's `lensmodel` program (2001) to fit models to our astrometry for WISE 2304-2214 and WISE 2344-3056 given in Tables 2 and 3.

5.1. WISE 2304-2214

For WISE 2304-2214 we used a singular isothermal ellipsoid. The generic expectation is that the quasar images will be micro-lensed (Witt, Mao and Schechter 1995) and we are reluctant to use their continuum flux ratos as constraints. But as this leaves the model underconstrained, we took the emission line flux ratio to be approximately unity and adopted this as a constraint.

The model puts the source $0\farcs17$ west and $1\farcs08$ north of image A and has a lens strength of $1\farcs04$. The model magnifications are, -2.6 and 2.6 for images A and B respectively. By contrast image A is 0.94 mag brighter than B in the r and i filters. We take this to be an indication of micro-lensing of the continuum. Image A is more likely to be micro-lensed than image B both because A is a saddle point (Schechter and Wambsganss 2002) and because B is more than twice as far from the lensing galaxy and passes through a lower surface density of stars.

The model ellipticty is 0.22 and is directed along P.A. $73\fdg0$ east of north. as compared to the observed ellipticity and orientation of 0.58 and $111\fdg4$. Shear of 0.1 from a galaxy $5''$ toward P.A.

30° from image B produces model with larger ellipticities that are more nearly aligned with the observation.

5.2. WISE 2344-3056

For WISE 2344-3056 we used a singular isothermal sphere with external shear to fit astrometric data in Table 2. As we do not detect the lensing galaxy, the center of the lens is left free and found to be $0\farcs436$ west and $0\farcs151$ north of image A. The model puts the source $0\farcs441$ west and $0\farcs153$ north of image A. The lens strength – which would be the radius of the Einstein ring were there no shear – is $0\farcs99$. The external shear is 0.063 and is directed along P.A. $-71\fdg5$. The signed magnifications for images A, B, C and D are, respectively, -6.8, 8.4, 8.6, -8.1.

6. Discussion

6.1. The method

We have searched for gravitationally lensed quasars by analyzing VST-ATLAS image cutouts of red WISE sources. Those that could be consistently split into two nearly pointlike objects with roughly constant flux ratios across multiple filters and quasar-like colors in those filters (specifically $u-g<-0.5$) were selected as candidates for followup spectroscopy and imaging. Three new lenses, two pairs of lensless twins, one binary quasar and two projected quasar pairs were found. Owing to bad weather during 2015 and 2016, only a fraction of the candidates (albeit some of the best) were observed.

The list of candidates is likely to increase considerably with a) completion of the ATLAS survey, b) application of the method to fainter WISE sources and c) incorporation of a more sophisticated scheme for gauging whether the *ugriz* colors of a particular pair of objects are quasar-like. The method could be extended to splitting sources into triples, with a primary goal of more readily identifying quadruply lensed quasars.

We encountered an unanticipated bottleneck in the speed with which the OmegaCam Science Archive can produce cutouts – something on the order of one cutout per second, far more than one might think necessary for retrieving 2500 pixels. The servers for the DES and KiDS surveys are not qualitatively faster. This casts a pall on programs that might require 10^7 or 10^8 cutouts. While it might be difficult to retool existing archives to speed up the process, we imagine that future systems will deal with such programs more efficiently.

Our method (modified for use with *grizY* photometry) is one of several now being used to search for lenses in the Dark Energy Survey (Agnello et al 2015; Ostrovski et al 2017), which ought to produce at least as many lensed quasars as ATLAS. As no one method will be perfect,

comparison of the results will shed light on their relative strengths and weaknesses.

6.2. Lensless Twins

The VST-ATLAS survey has better seeing than SDSS, allowing, in principle, the discovery of less widely separated lensed quasars. But the galaxies that produce close pairs are fainter than those that produce wide pairs and are more crowded by the lensed quasar images, making it more difficult to identify them.

We have argued that it is premature to classify either of our "lensless twin" quasars as binary quasars – fraternal twins – despite the fact that no lensing galaxy has as yet been identified. In Figure 8 we show the two systems, with the component spectra shifted to overlap. For WISE 0326-3122 the agreement is nearly perfect, while for WISE 1051-1142 the differences are consistent with what one would expect for a micro-lensed system. We note that WISE 2329-1258 was at first classified as a lensless twin system, but in the time since the original submission of this paper has been reclassified as lensed quasar with the detection of a lensing galaxy by other investigators.

With sufficiently deep direct images in sufficiently good seeing one can set upper limits on the lensing galaxy that rule out the lensing hypothesis, but only with extensive modeling of lensing scenarios. If higher signal-to-noise spectra, or spectra at other wavelengths were to show significant differences in the line profiles, they would again rule out the lensing hypothesis. Confirmation of the lensing hypothesis might come either from identification of the lensing galaxy or from correlated variations in the fluxes, as might be obtained from synoptic observations with the LSST.

7. Summary

We have analyzed images from the VST ATLAS survey to identify candidate gravitationally lensed quasar systems in a sample of WISE sources with $W1 - W2 > 0.7$. Results from followup spectroscopy with the Baade 6.5 m telscope are presented for eight systems. One of these is a quadruply lensed quasar, and two are doubly lensed systems. Two are projected superpositions of quasars at two different redshifts, and one appears to be a pair of distinct quasars at the same redshift. In two systems the component spectra are consistent with the lensing hypothesis, after allowing for micro-lensing. But as no lensing galaxy is detected in these two, we classify them as lensless twins. More extensive observations are needed to establish whether they are lensed quasars or physical binaries.

REFERENCES

Agnello, A., Treu, T., Ostrovski, F., et al. 2015, MNRAS, 454, 1260

Agol, E., & Krolik, J. 1999, ApJ, 524, 49

Blackburne, J. A., Pooley, D., Rappaport, S., & Schechter, P. L. 2011, ApJ, 729, 34

Courbin, F., Lidman, C., & Magain, P. 1998, A&A, 330, 57

Cross, N. J. G., Collins, R. S., Mann, R. G., et al. 2012, A&A, 548, A119

Dressler, A., Bigelow, B., Hare, T., et al. 2011, PASP, 123, 288

Hambly, N. C., Collins, R. S., Cross, N. J. G., et al. 2008, MNRAS, 384, 637

Hennawi, J. F., Strauss, M. A., Oguri, M., et al. 2006, AJ, 131, 1

Inada, N., Oguri, M., Shin, M.-S., et al. 2012, AJ, 143, 119

Jiménez-Vicente, J., Mediavilla, E., Kochanek, C. S., & Muñoz, J. A. 2015, ApJ, 799, 149

Keeton, C. R. 2001, arXiv:astro-ph/0102340

Kochanek, C. S., Falco, E. E., & Muñoz, J. A. 1999, ApJ, 510, 590

Lidman, C., Courbin, F., Kneib, J.-P., et al. 2000, A&A, 364, L62

Mortlock, D. J., Webster, R. L., & Francis, P. J. 1999, MNRAS, 309, 836

Ostrovski, F., McMahon, R. G., Connolly, A. J., et al. 2017, MNRAS, 465, 4325

Pooley, D., Blackburne, J. A., Rappaport, S., & Schechter, P. L. 2007, ApJ, 661, 19

Pooley, D., Rappaport, S., Blackburne, J. A., Schechter, P. L., & Wambsganss, J. 2012, ApJ, 744, 111

Rauch, K. P., & Blandford, R. D. 1991, ApJ, 381, L39

Remy, M., Claeskens, J.-F., Surdej, J., et al. 1998, New A, 3, 379

Richards, G. T., Fan, X., Schneider, D. P., et al. 2001, AJ, 121, 2308

Schechter, P. L., Mateo, M., & Saha, A. 1993, PASP, 105, 1342

Schechter, P. L., & Wambsganss, J. 2002, ApJ, 580, 685

Schechter, P. L., & Wambsganss, J. 2004, in IAU Symposium, Vol. 220, Dark Matter in Galaxies, ed. S. Ryder, D. Pisano, M. Walker, & K. Freeman, 103–+

Shanks, T., Metcalfe, N., Chehade, B., et al. 2015, MNRAS, 451, 4238

Sérsic, J. L. 1963, Boletin de la Asociacion Argentina de Astronomia La Plata Argentina, 6, 41

Stern, D., Assef, R. J., Benford, D. J., et al. 2012, ApJ, 753, 30

Treu, T., & Marshall, P. J. 2016, A&A Rev., 24, #11

Witt, H. J., Mao, S., & Schechter, P. L. 1995, ApJ, 443, 18

Wisotzki, L., Koehler, T., Kayser, R., & Reimers, D. 1993, A&A, 278, L15

Wisotzki, L., Koehler, T., Ikonomou, M., & Reimers, D. 1995, A&A, 297, L59

Wright, E. L., Eisenhardt, P. R. M., Mainzer, A. K., et al. 2010, AJ, 140, 1868-1881

This preprint was prepared with the AAS LaTeX macros v5.2.

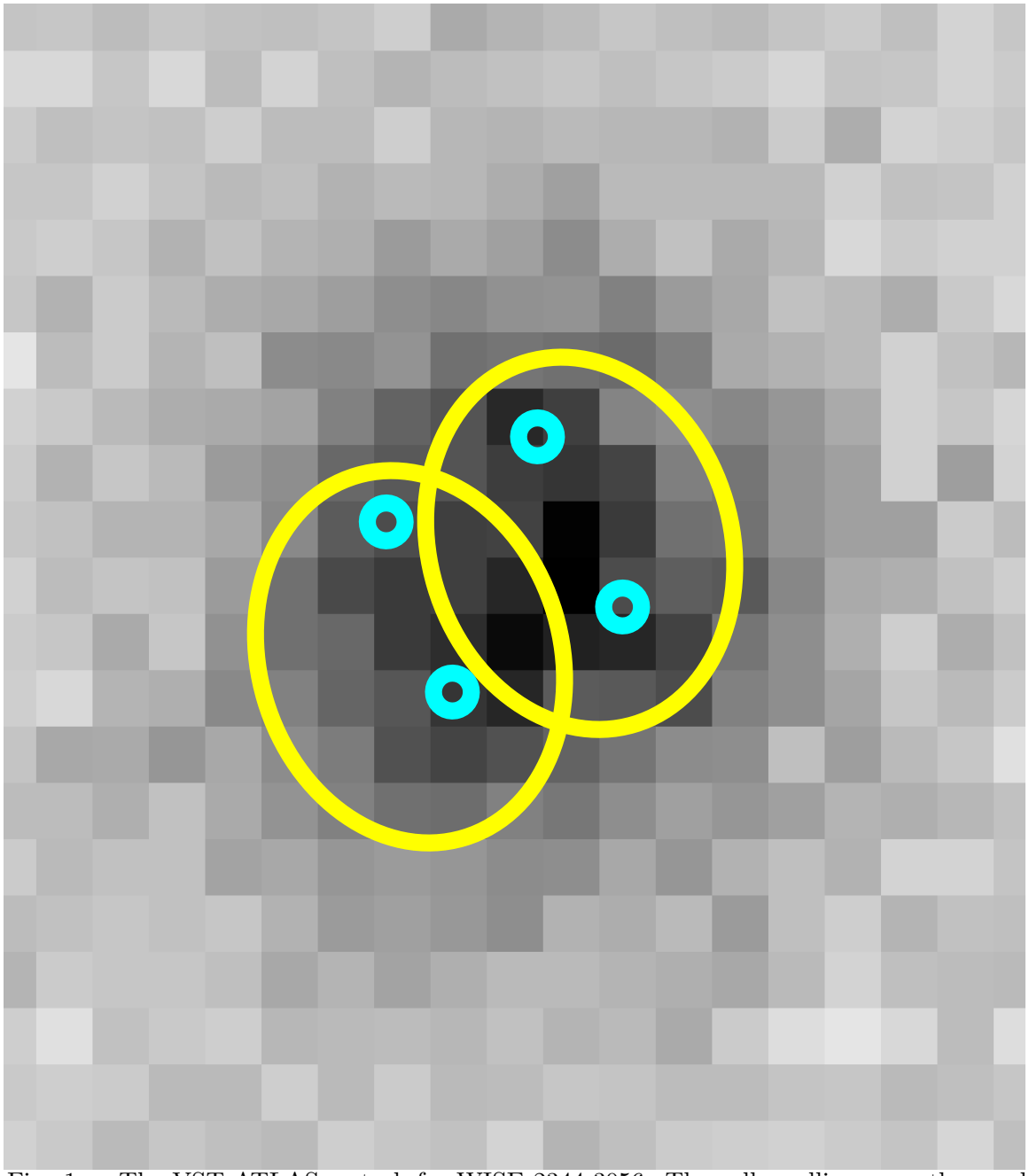

Fig. 1.— The VST-ATLAS g stack for WISE 2344-3056. The yellow ellipses are the result of our anchor splitting of this source. The blue circles are at the positions of the four images (D, C, B and A from left to right) identified with IMACS. The scale is $0\farcs213$ per pixel. North is up and East is to the right.

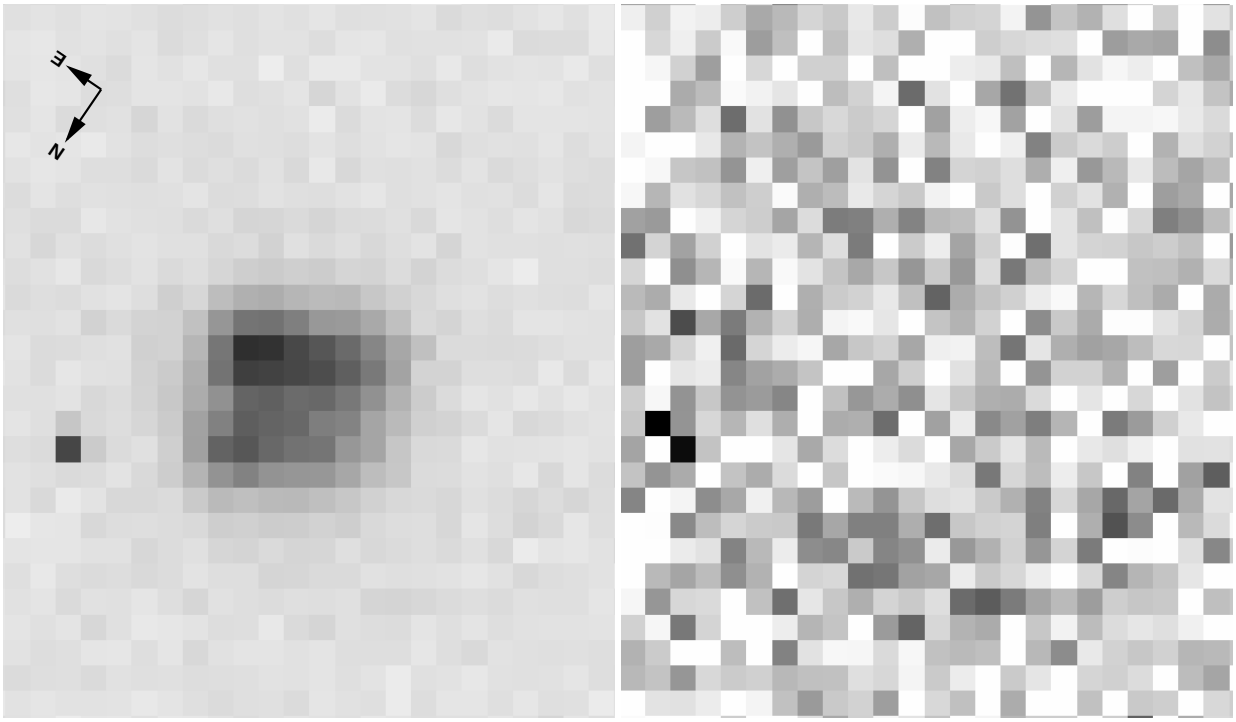

Fig. 2.— Left: A 60s i exposure of WISE 2344-3056 taken with IMACS in 0.″55 seeing. Right: the same exposure, with four point sources subtracted, at 10 times higher contrast. The scale is 0.″200 per pixel

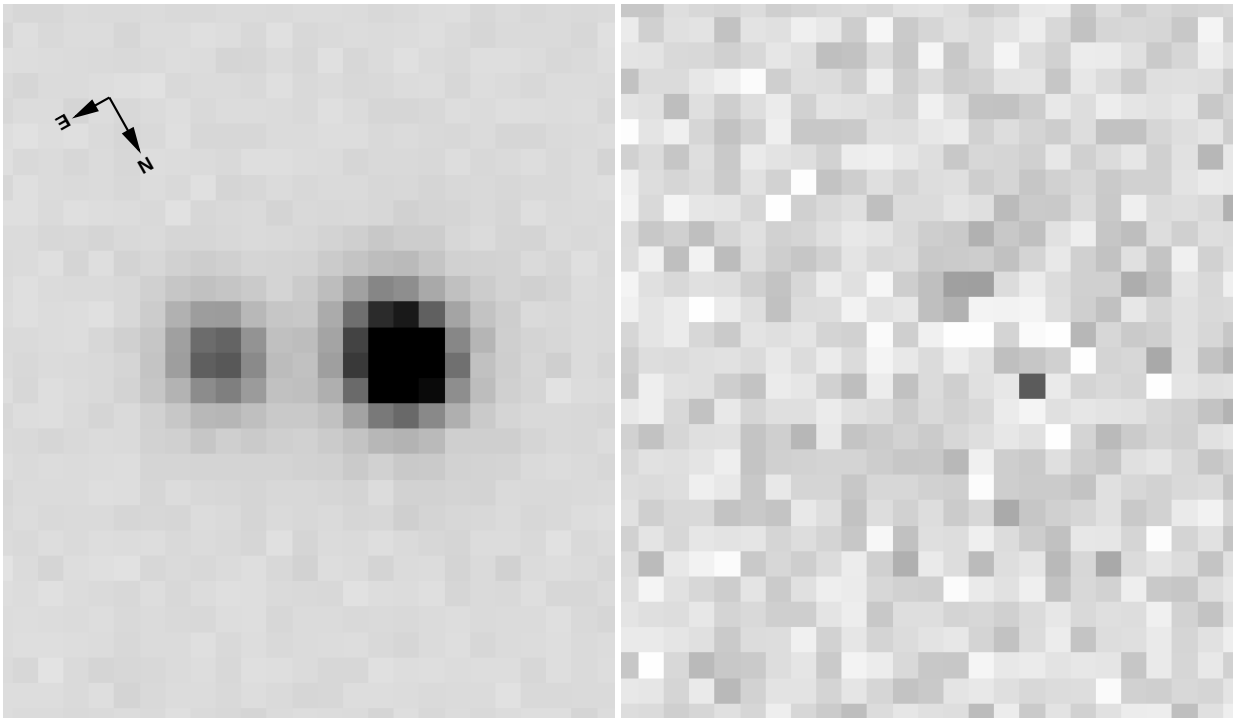

Fig. 3.— Left: A 30s Sloan r exposure of WISE 0326-3122 in 0.″64 seeing. Right: the same exposure, with two point sources subtracted, at 5 times higher contrast. The scale is 0.″200 per pixel.

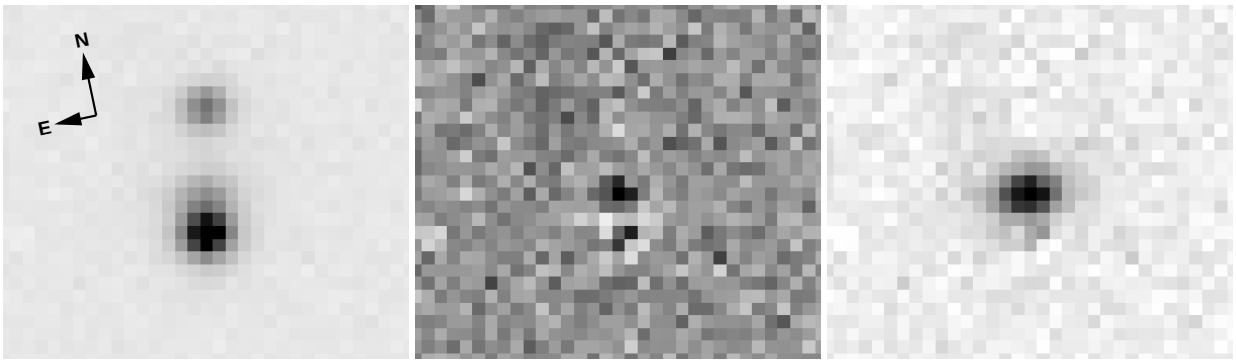

Fig. 4.— Left: A 60s Sloan i exposure of WISE 2304-2214 in 0.″64 seeing. Center: the same exposure, with two point sources and an extended source subtracted, at 10 times higher contrast. Right: the same exposure with only the point sources subtracted, at 4 times higher contrast. The scale is 0.″221 per pixel.

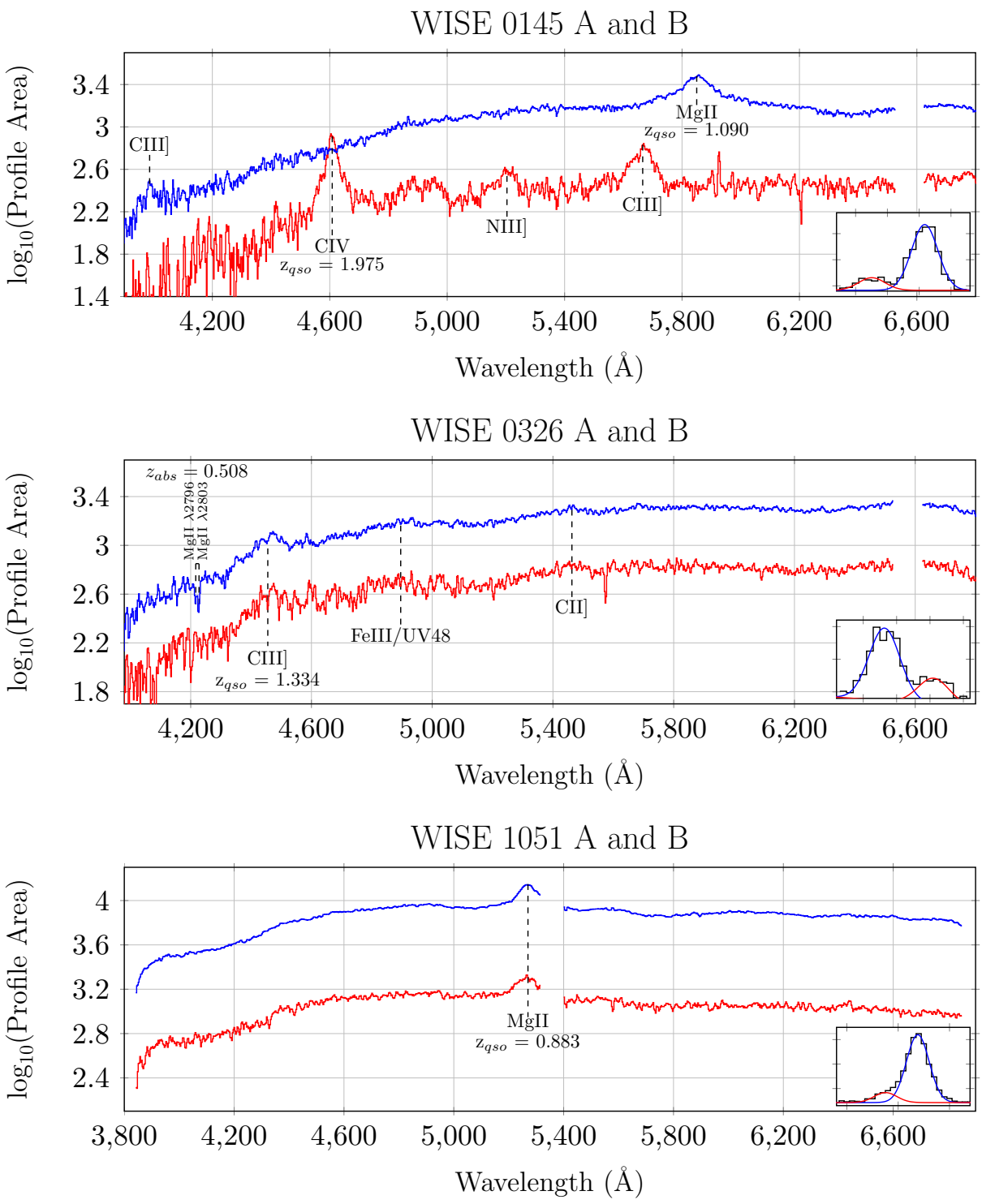

Fig. 5.— IMACS spectra of WISE 0145-1327, WISE 0326-3122, and WISE 1051-1142. Image A is brighter than image B.

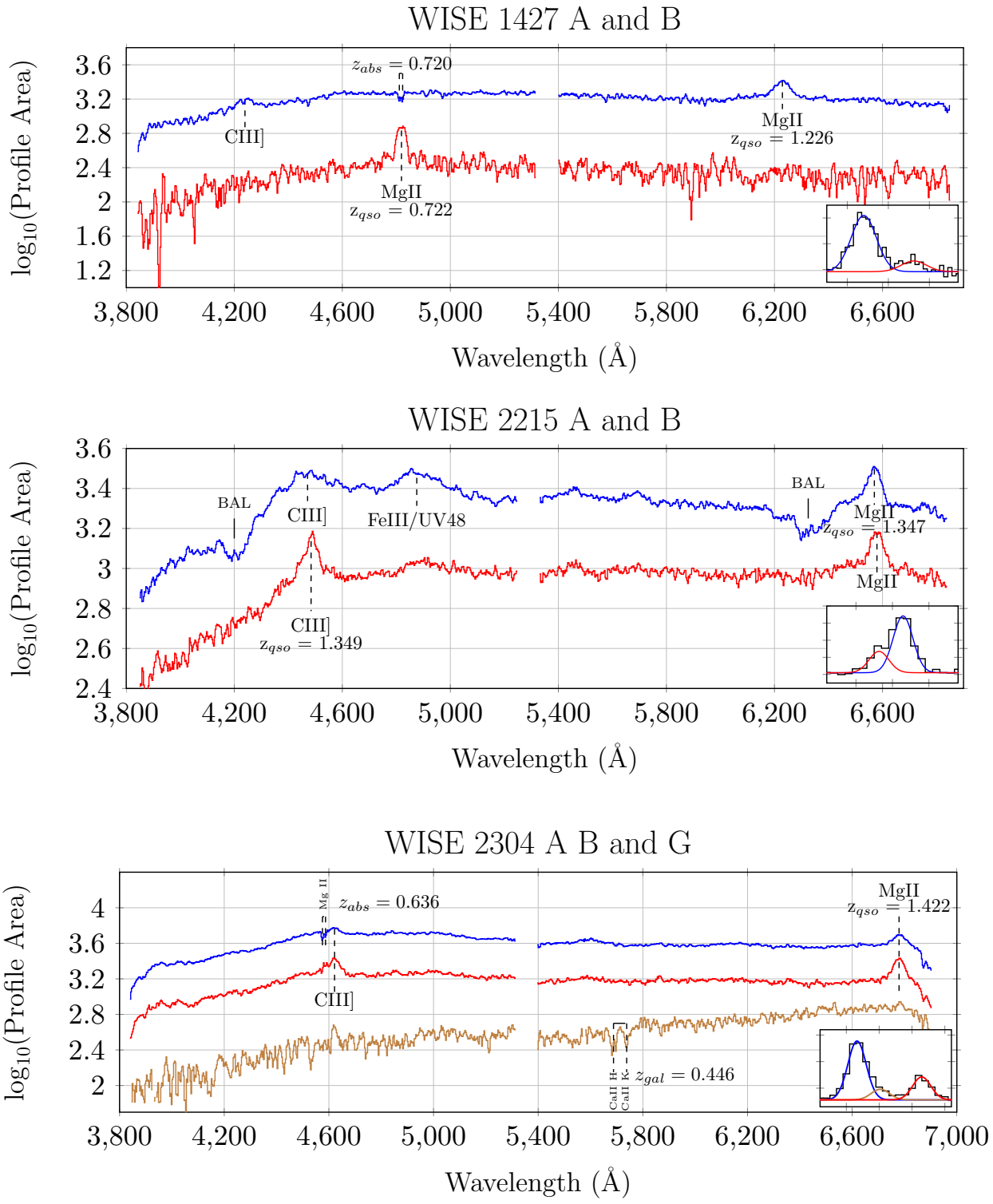

Fig. 6.— IMACS spectra of WISE 1427-0715 and WISE 2215-3056 and WISE 2304-2214. Image A is brighter than image B.

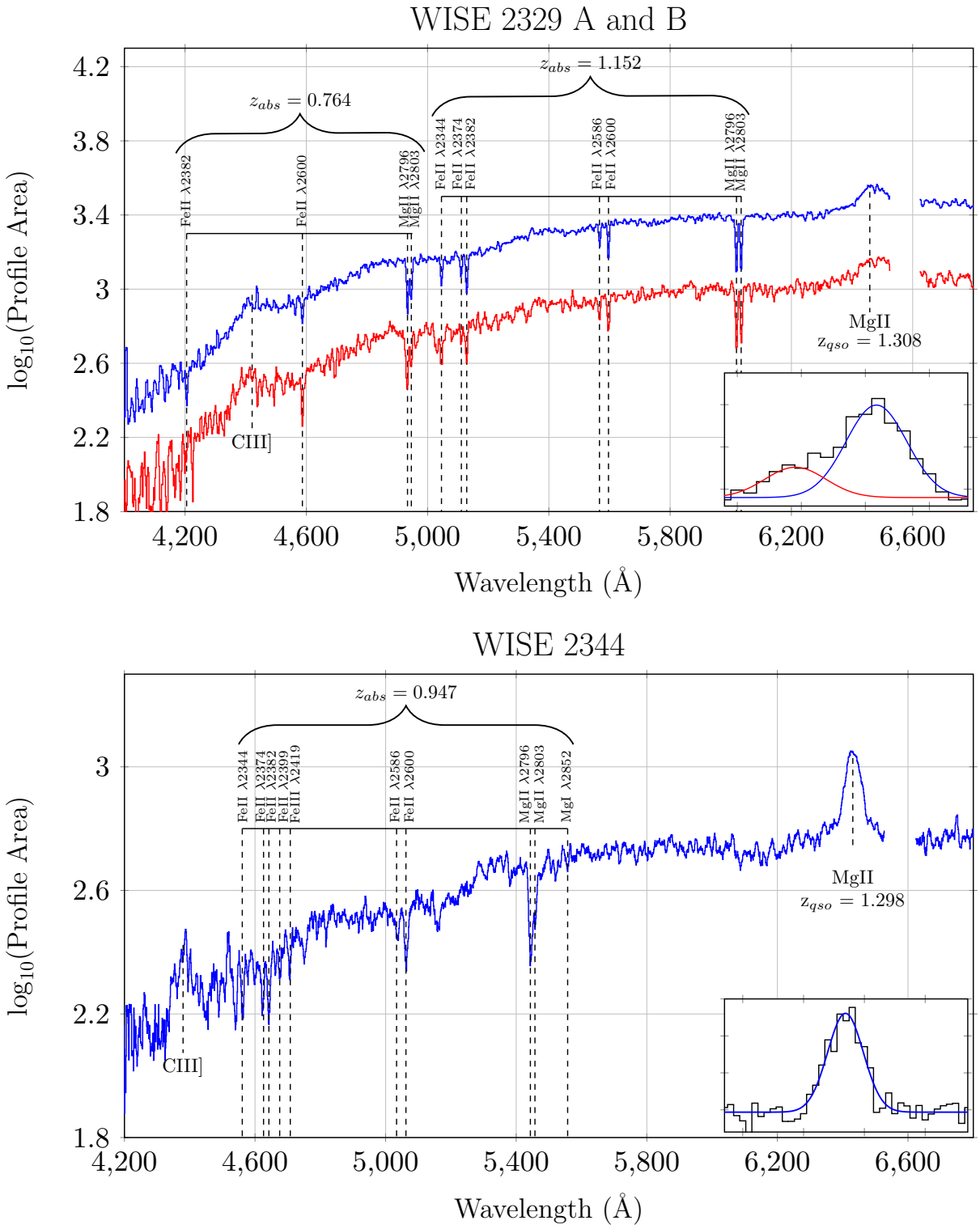

Fig. 7.— IMACS spectra of WISE 2329-1258 A (upper) and B (lower) and WISE 2344-3056, taken with IMACS

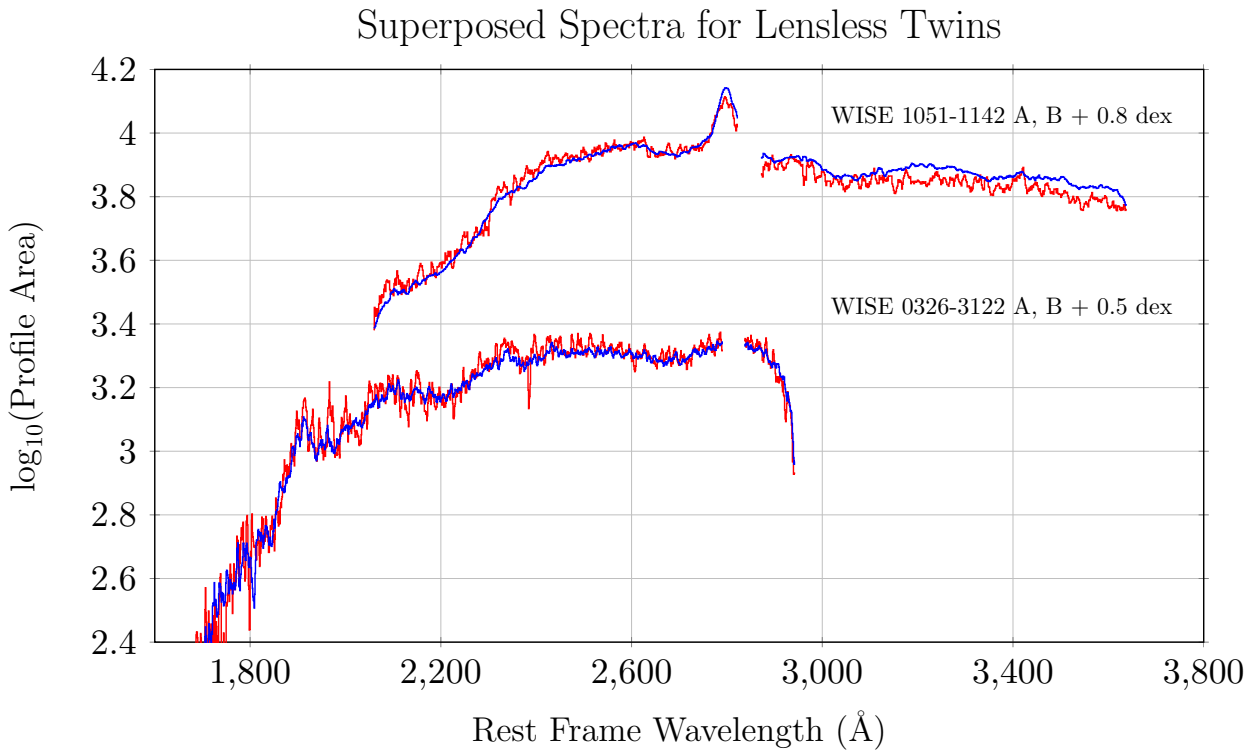

Fig. 8.— Rest frame spectra of WISE 0326-3122 and WISE 1051-1142 with the *A* and *B* components superposed.

Table 1. Spectroscopic Observations of Lensed Quasar Candidates

name	R.A. Dec.	$\Delta\theta$ P.A.	i^*_A i^*_B	score $(u-g)^\dagger$	camera exp.	description redshift(A/B)
WISE 0145-1327	01 45 25.3	1.″68	19.25	0.39	f/2	projected
	−13 27 25	5°	20.59	-1.01	1200s	1.09/1.97
WISE 0326-3122	03 26 06.8	1.″43	19.49	0.60	f/2	lensless twins
	−31 22 54	−60°	20.56	-1.17	1200s	1.34
WISE 1051-1142	10 51 41.9	1.″47	17.25	0.50	f/4	lensless twins
	−11 42 39	−5°	19.39	-0.89	900s	0.88
WISE 1427-0715	14 27 04.8	2.″80	18.92	0.49	f/4	projected
	−07 15 56	9°	20.32	-0.73	900s	1.23/0.72
WISE 2215-3056	22 15 25.6	0.″71	18.31	0.29	f/4	binary
	−30 56 35	−41°	19.07	-0.61	900s	1.34
WISE 2304-2214	23 04 25.3	2.″19	19.57	0.58	f/4	lensed
	−22 14 46	−11°	20.50	-1.37	1800s	1.42
WISE 2329-1258	23 29 57.9	1.″27	17.63	0.96	f/2	lensed
	−12 58 59	46°	18.60	-0.82	600s	1.314
WISE 2344-3056	23 44 17.0	2.″18	20.31‡	0.44	f/2	quadruple
	−30 56 26	−12°	20.63‡	-0.63	900s	1.298

*magnitudes for A and B components derived from catalogued ATLAS Petrosian AB magnitudes and constrained separation flux ratios,.

†$u-g$ colors are in the Vega-like system of the ATLAS FITS headers

‡$i_C = 20.71$ and $i_D = 21.12$

Table 2. Astrometry* and Photometry for WISE 2344-3056

image	$\Delta\alpha$	$\Delta\delta$	i
A	$0\farcs000$	$0\farcs000$	20.31
B	-$0\farcs304$	$0\farcs665$	20.63
C	-$0\farcs641$	-$0\farcs337$	20.71
D	-$0\farcs886$	$0\farcs293$	21.12

*Positions in arcseconds relative to $\alpha_A = 23^h44^m16\farcs995$ and $\delta_A = -30°56'26\farcs22$

Table 3. Astrometry* and Photometry† for WISE 2304-2214

image	$\Delta\alpha$	$\Delta\delta$	r	i
A	$0\farcs000$	$0\farcs000$	19.52	19.57
B	-$0\farcs431$	$2\farcs145$	20.46	20.50
G	-$0\farcs093$	$0\farcs673$	21.48	20.65

*Positions in arcseconds relative to $\alpha_A = 23^h04^m25\farcs348$ and $\delta_A = -22°14'46\farcs95$

†magnitudes from three component fits to Magellan images with scale set by ATLAS AB magnitudes for template stars